Single-molecule Force Spectroscopy Measurements of "Hydrophobic Bond" between Tethered Hexadecane Molecules

Chad Ray, Jason R. Brown, and Boris B. Akhremitchev*

Department of Chemistry, Duke University, Durham, North Carolina 27708

Received: June 7, 2006; In Final Form: July 16, 2006

The hydrophobic effect is important for many biological and technological processes. Despite progress in theory, experimental data clarifying water structure and the interaction between hydrophobic solutes at the nanometer scale are scarce due to the very low solubility of hydrophobic species. This article describes an AFM single molecule force spectroscopy method to probe the interaction between molecules with low solubility and reports measurements of the strength and the length scale of the "hydrophobic bond" between hexadecane molecules. Hexadecane molecules are tethered by flexible poly(ethylene glycol) linkers to AFM probes and substrates, removing the aggregation state uncertainty of solution-based approaches as well as spurious surface effects. A shorter hydrophilic polymer layer is added to increase the accessibility of hydrophobic molecules for the force spectroscopy measurements. Statistical analysis of the rupture forces yields a barrier width of 0.24 nm, and a dissociation rate of 1.1 s^{-1}. The results of single molecule measurements are related to the theoretical predictions of the free energy of cavitation in water and to the empirical model of micellization of nonionic surfactants. It is estimated that approximately one-quarter of each molecule's surface is hydrated during forced dissociation, consistent with an extended (nonglobular) conformation of the hexadecane molecules in the dimer.

Introduction

The hydrophobic interaction is an important participant in the process of folding biological macromolecules and in the assembly of supramolecular structures such as biological membranes in an aqueous environment.[1−5] The nature of the hydrophobic effect is related to the disruption of the hydrogen-bonding network in water. It has been predicted that details of the water structure around hydrophobic species depend on the size of the hydrophobic solute with predicted depletion of the water density starting at the hydrophobic solute dimension above ∼1 nm.[6,7] Interpretation of experimental results that indicate a decrease in the water density at hydrophobic surfaces and formation of nano-bubbles are still debated.[8−11] Experimental techniques such as NMR, FTIR, and chromatographic methods have limitations in measuring size-dependent solvation due to the low solubility of relatively large hydrophobic molecules[12] and often cannot distinguish between dimerization and oligomerization of hydrophobic species. Experimental methods that study hydrophobic interactions directly by measuring forces between hydrophobic surfaces[13−15] are often limited to large length scales. Atomic force microscopy (AFM) measurements approach the nanometer length scale, although such measurements might contain artifacts due to surface contamination by polymeric species.[11] Here we report force spectroscopy measurements with AFM of forces between single hydrophobic molecules (hexadecane) tethered to solid surfaces via hydrophilic polymeric linkers.[16] These measurements bring the experimental scale of measuring hydrophobic effects to the nanometer level while avoiding the contamination problem. This study initiates a series of investigations that aim to test current theoretical predictions for hydrophobic hydration of interacting solutes by direct measurements of rupture forces between single molecules. The size [6,7] dependence is of particular interest, as is the temperature dependence [17] of the transition length scale, because these dependencies correspond to fundamental changes in the nature of water's structure at the hydrophobic surfaces.

In force spectroscopy, the detection probability of binding events between the tethered molecules relies on rates of collision and association between the tether-end molecules. In the case of low activity of the attached molecules, the ends of tethers remain adsorbed at the surface, therefore, dramatically decreasing the probability of detecting the events of intermolecular association. When tethered molecules remain adsorbed to the surface, it is possible to "activate" an interaction by bringing the bound molecules together during the mechanical contact between the probe and the surface (See Figure 1). When intermolecular interactions are stronger than the adsorption forces, the surface-bound molecules can be lifted from the surface, permitting measurement of interactions away from the substrates at the probe-sample separation approximately equal to the sum of the tether lengths.[16,18] The probability of a surface encounter between bound molecules depends on the probe-surface contact area and on the grafting density. Therefore, it is expected that using softer surfaces that provide larger contact area should increase the probability of detecting the single-molecule binding events. One way to form a soft interface is by adding a layer of shorter hydrophilic polymer that forces the tether-end molecule out into solution.[19,20] Adding a non-functional poly(ethylene glycol) (PEG) layer in order to dilute the surface concentration of interacting molecules is reported in the literature.[16,21] The PEG underlayer is used here, not only to dilute the grafted molecules, but primarily to increase the detection probability of binding events at the double-tether length. The shorter polymer fills the space close to the surface, establishing a repulsive barrier that pushes the

* Corresponding author phone: (919) 660-1648; fax: (919) 660-1605; e-mail: boris.a@duke.edu.

10.1021/jp063517r CCC: $33.50
Published on Web 08/17/2006

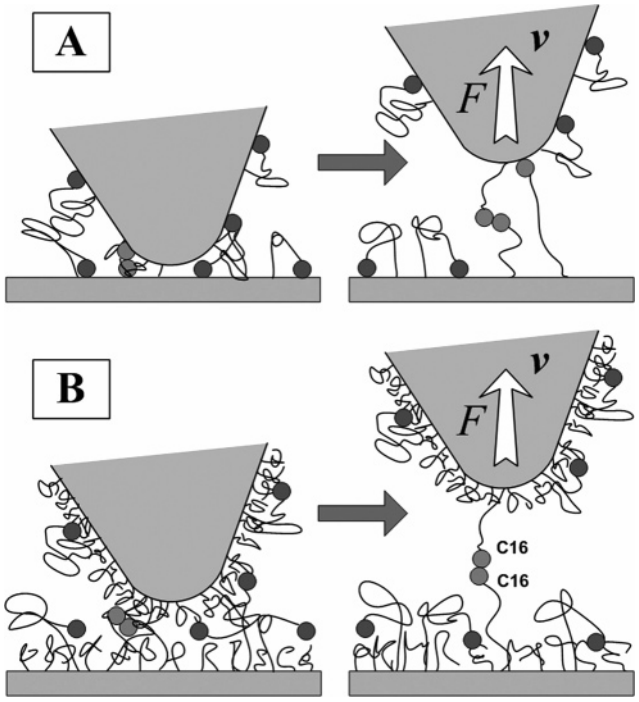

Figure 1. Cartoons showing functionalized tip and surface interaction. Panel A shows the case without a shorter polymer layer where the low activity tether-end molecules phase separate from the bulk solution. The single tether interactions with the substrate are not hindered (as indicated in the figure), and an example of a double tether interaction being activated by the contact of the tip with the surface is shown. Panel B shows the case with added shorter polymer layer. As predicted by simulations,[19,20] the tether-end molecules are shown sterically held off of the surface, facilitating the double tether interactions and hindering single tether interactions.

longer tethers and its attached end group out into solution and prevents nonspecific adsorption of the hydrophobic end-groups to the substrate, reducing the probability of phase separation by the attached hydrophobic end-group.[19,20] The combination of these effects increases the interaction area between the tip and the surface, facilitating creation and detection of intermolecular binding events.

Experimental Section

Sample Preparation. Samples were prepared by an approach similar to the previously reported method.[16,21] All chemicals were purchased from Aldrich, unless specified. The reaction vessels used for the sample preparation reactions were either glass or Teflon. Briefly, cleaned glass cover slips (Fisher Scientific) and silicon nitride AFM probes (Veeco, NP series probes) were aminated with ethanolamine in dry DMSO for 24 h.[22] α-N-Hydroxysuccinimide-ω-maleimide-poly-(ethylene glycol) (NHS−PEG−MD) (Nektar Therapeutics, Huntsville, AL) linkers with mass-averaged molecular weight of 3535 Da are covalently attached to the surface through the NHS-amine reaction and to 1-hexadecanthiol through the reaction of the terminal thiol with the PEG's MD terminal.[23] Both of these reactions are carried out simultaneously for 24 h in anhydrous toluene with 5% pyridine (v/v). Control measurements use samples that include grafted PEG tethers reacted with 2-mercaptoethanol instead of 1-hexadecanethiol. The second reaction to the surface amines is then performed on one set of AFM probes and glass surfaces with α-N-hydroxysuccinimide-ω-ethyl ether-poly(ethylene glycol) (SS−PEG) (Polysciences, Inc., Warrington, PA) with a molecular weight of 1900 Da. This fills in the remaining surface area below the longer PEG tethers to hinder tethered hexadecanes from phase separating onto the solid substrate. This reaction is performed for 48 h in toluene with 10% pyridine. A final reaction with N-hydroxysuccinimide acetoacetate in 60% toluene, 30% DMSO, and 10% pyridine is performed overnight to block any remaining amines. The samples are then cleaned in water, toluene, DMF, and ethanol to remove physisorbed molecules and used immediately after preparation. Measurements were performed with the three combinations of substrates and AFM probes: both surfaces contain tethered hexadecane but without an additional PEG layer, surfaces contain tethered hexadecane with an additional PEG layer, and the control set with one surface containing hexadecane and another containing ethoxy-capped PEG tethers.

Data Collection. Force spectroscopy measurements were performed with Asylum Research MFP3D AFM (Santa Barbara, CA) using modified silicon nitride probes (Veeco, Santa Barbara, CA) with spring constants of 70 pN/nm and 80 pN/nm. Spring constants are found using the thermal noise analysis method. Each cantilever is used for an entire set of data because the experimental error in spring constant has ∼20% error.[24] The experimental procedure and the data processing were described previously,[16] and details of the data manipulation are described in the Supporting Information. Experiments were conducted in pH 7 phosphate buffer and at different temperatures. A custom-made temperature stage is used to set the temperature and a custom-made O-ring is used to reduce evaporation of the phosphate buffer when the AFM probe is engaged over the sample. A total of 4096 force curves were collected in each measurement performed at a particular value of temperature and probe velocity. The interaction between tethered molecules was initiated by bringing two surfaces together. Rupture forces were detected during the reverse motion of the probe. Probe position was raster scanned over the samples surface after each force plot measurement to obtain a good statistical average over the sample's surface. Force−distance curves collected at each probe position were digitally stored for the subsequent analysis.

Data Analysis. The double tether approach[16,18,21] is used to distinguish the rupture events between the tethered molecules from the ruptures between the tethered molecule and the substrate surface. Force−distance curves reveal that rupture events occur at different probe positions above the sample surface. Prior to rupture events, the polymer tethers are stretched with end-to-end distances far exceeding the average distances found at thermal equilibrium. This stretching results in a characteristic force-separation dependence that is used as an initial selection criterion in data analysis. Mass-spectroscopy of PEG linkers reveals a molecular weight distribution from 3200 to 4100 Da at half-maximum.[16] Long tethers are used to clearly identify rupture events between tethered molecules. Rupture events that correspond to the sum of the tether's stretched lengths (contour lengths ranging from 35 to 70 nm) were used in statistical analysis of rupture forces. The indicated range includes the polydispersity of tethers as well as conformational transition of PEG tethers under force.[25] An extended freely jointed chain (FJC) model that includes a conformational transition of PEG linkers[25] was fit to each tether-stretching event (full details provided in the Supporting Information).

Results and Discussion

Detection Capability. Panel A in Figure 2 shows a characteristic force-separation event detected at the double-tether length with a superimposed fit by an extended freely jointed chain (FJC) model.[16,25] The PEG linker stretching event is character-

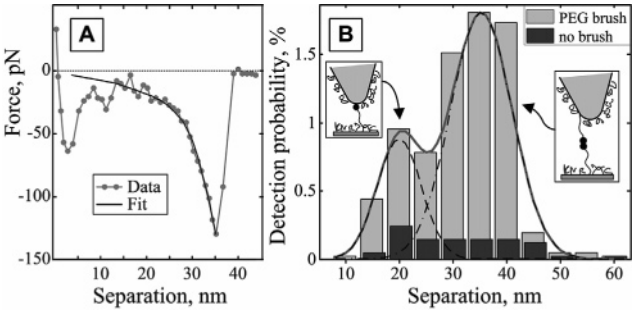

Figure 2. Panel A shows a characteristic force-separation dependence with a superimposed fit by the extended FJC model.[16,25] The fit gives a Kuhn length value of 0.55 nm and a contour length of 43 nm. Rupture occurs at approximately the double tether length (at 35 nm), indicating unbinding between solubilized species. Panel B shows the detection probability of the rupture events at different probe-sample separations for samples with and without additional PEG layer grafted at the surface, as indicated in the figure. The first peak at ~20 nm corresponds to stretching of the single tether; the second peak at ~35 nm corresponds to the double-tether detection of rupture events away from the surface. Data shown in this figure were collected at 35 °C.

istically nonlinear and is well fit by the extended FJC model, indicating that these events are indeed the expected polymer stretching events. All of the force curves that exhibit rupture events at separations greater than 20 nm were fit by the extended FJC model,[25] finding the average Kuhn length of 0.56 ± 0.27 nm and the average contour length of 57 ± 14 nm. Rupture events that are not well fit by the extended FJC model (less than 10% of the total rupture events) are excluded from further analysis because of identification uncertainty. The average contour length corresponds to the molecular weight of 7.0 kDa, which is very close to twice the average molecular weight of the individual PEG tether.[16,25]

Measurements between samples with an added short PEG layer exhibited consistently higher probability of the double-tether detection as shown in Panel B of Figure 2. This panel shows that adding a soft PEG layer increased the probability of detecting rupture events 7-fold; more importantly most of events are detected at the desired double tether length. It was noted that the high probability of detecting rupture events at the double tether length diminished significantly with long exposure time of the sample to water. This decrease can be attributed to the burying of hydrophobic hexadecane molecules inside the PEG surface layer.

Control experiments with empty (ethoxy-capped) linker showed, on average, approximately five rupture events at the double-tether length out of four thousand attempts. This number is negligible in comparison with the number of events detected with normal samples (usually 3−5% of all attempts). The results with empty linker confirm that the detected rupture events are due to unbinding between the tethered alkanes.

Loading Rate Dependence. Loading rate-dependent experiments were performed at 30 °C. Rupture forces and loading rates were extracted from the force-separation data.[16] Figure 3 shows the scatter plot of the rupture force dependence on the loading rate. The dependence of the rupture force on the logarithm of the loading rate was fit by a line to obtain the distance from the equilibrium to the transition state (further called barrier width for brevity) along the direction of forced dissociation.[26,27]

The fit line has slope of 18 ± 2 pN, [28] this slope corresponds to a barrier width ($x^{\ddagger}$) of 0.24 ± 0.03 nm according to $x^{\ddagger} = k_B T/s$ where T is the temperature, k_B is the Boltzmann's constant, and s is the slope of the best-fit line in semilog coordinates. It has to be noted that this value is probably an underestimation of the actual barrier width, which could be nearly 50% higher due to loading the molecular bond with a nonconstant loading rate.[26] At the same time, limited force sensitivity can cause some overestimation of $x^{\ddagger}$. The measured value of $x^{\ddagger}$ falls between calculated values for small and large solutes (separation of ~1.5 Å from the contact position to the first maximum of the potential energy of mean force for spheres with diameter of 5 Å [29] and barrier width of ~3 Å calculated for larger surfaces[30]) and is close to the barrier width of ~2.3 Å calculated for separation between two fullerenes.[31] The effective radius of hydrocarbons used here is close to the crossover length scale of hydrophobic hydration.[32] At this length scale the barrier width is expected to vary with the size of hydrophobic molecules. The barrier width dependence on the size of alkanes will be a subject of future studies.

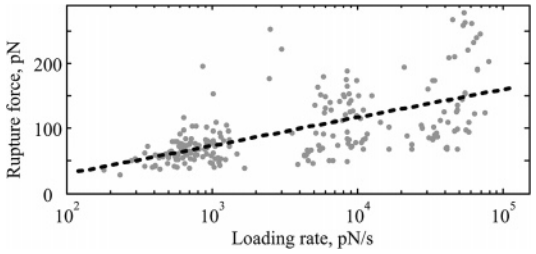

Figure 3. Figure shows a scatter plot of measured rupture forces at different loading rates. Loading rate was determined from the slope of the force vs time dependence immediately preceding the rupture event. The dashed line shows the linear fit to the data in semilog coordinates.

The dissociation rate at zero force (K_d^0) can be estimated from the intercept of the linear fit of force vs loading rate in semilog coordinates. Data shown in Figure 3 gives loading rate of log (K_d^0) = 0 ± 1 s^{-1} (K_d^0 = 1.1 s^{-1}). It has to be noted that besides the large random error due to dispersion in the data, estimated rate also contains error due to the essentially nonconstant loading rate during pulling that results from stretching of the polymeric linker, behaving as a nonlinear entropic spring.[26,27] Moreover, since the slope of the force vs log(loading rate) dependence also contains error, the error in the reaction rate could be large, and according to Monte Carlo simulations, it can be several-fold.[26] Analysis of the systematic errors in the barrier width and in the dissociation rate from force spectroscopy measurements will be a subject of a separate study.

With the known dissociation rate Arrhenius' equation can be used to estimate activation energy $\Delta G^{\ddagger}$:

$$K_d^0 = f \cdot e^{-\Delta G^{\ddagger}/R \cdot T} \qquad (1)$$

Here K_d^0 is the dissociation rate, R is the gas constant, T is temperature, and f is the pre-factor. The pre-factor can be estimated approximately equal to 10^7 s^{-1} using experimental data for the cyclization of peptides with similar size to two hexadecane molecules.[33] This gives $\Delta G^{\ddagger}$ = 41 ± 6 kJ mol^{-1}. It can be noted that, according to molecular dynamics simulations,[8,30] the difference between activation energy $\Delta G^{\ddagger}$ and dissociation energy ΔG_d is approximately 10%, therefore, the value for $\Delta G^{\ddagger}$ obtained above can be compared with the difference in the solvation free energy of joined vs separated hydrocarbons and to the free energy of hydration. The difference in this energy can be approximated by the difference in cavitation energies,[6,34] therefore

$$\Delta G_d \cong 2\Delta G^{\text{cavitation}}(R_{c,1}) - \Delta G^{\text{cavitation}}(R_{c,2}) \qquad (2)$$

where $\Delta G^{\text{cavitation}}(R_c)$ is the cavitation energy of a sphere with

the cavity radius R_c (calculated using the molar volume V of solute as $R_c = [3V/4\pi]^{1/3} + \sigma_w/2$), $R_{c,1}$ is the radius of the cavity that includes one hexadecane molecule, $R_{c,2}$ is the radius of the cavity that includes two molecules, and σ_w is the hard-sphere diameter of water.[17,34] Cavitation energies can be calculated using different analytical models,[17,34] and the radii of cavities determined from the hexadecane molar volume of 0.30 cubic nm [35,36] and a hard-sphere diameter of water of 0.27 ± 0.01 nm.[17,34] The resulting free energy according to the cavity equation of state[17] is $\Delta G_d \approx 50 \pm 2$ kJ·mol^{-1}; the calculation is according to the analytical interpolation of the free energy perturbation model,[34] and the same radii of cavities gives $\Delta G_d \approx 58 \pm 2$ kJ·mol^{-1}. These values noticeably exceed $\Delta G^{\ddagger}$ estimated above from force-spectroscopy measurements. One possible explanation of this discrepancy is that the linear chain hexadecane in water adopts a nonglobular like conformation,[6,37] and thus spherical cavity models overestimate the dissociation energy.

The measured activation energy of 41 ± 6 kJ·mol^{-1} can be related to the number of fully hydrated carbons in the hydrocarbon chain using the hydrocarbon solubility data.[38] The free energy of hydration can be calculated according to $\Delta\mu_{hydration}^{\circ} = -10.2-3.70\cdot n_C$ [kJ/mol], thus the number of hydrated carbons upon separation of the two hexadecanes is 8 ± 2. This number indicates that approximately 1/4 of each hexadecane surface gets hydrated upon dissociation and this in turn implies that in the dimeric state hexadecane molecules are likely to have an extended nonglobular conformation as usually alkanes of this size and shorter have in the monomeric state in water.[6,37,39]

In the above analysis, the effect of PEG linkers that tether hexadecanes to surfaces on ΔG_d was not considered. To justify this approximation, a comparison to the empirical model that describes aggregation of alkyl ethoxides can be made.[40] Then applying force to separate two grafted hexadecane hydrocarbons, PEG linkers are stretched and most likely they do not contribute to the energy difference between associated and dissociated states because before, during, and immediately after the rupture between the molecules the tethers remain significantly stretched and do not interact with each other.[40] The critical micelle concentration (CMC) can be calculated according to the empirical model,[41] and the molar fraction for 16-carbon alkyl head without the PEG tail is $X_{CMC} = 6.1 \times 10^{-9}$. According to the thermodynamic model of micellization,[42] the overall energy gain per aggregated molecule is equal to $\alpha = RT\ln(X_{CMC})$. For a hexadecane head without an ethoxide tail α becomes −47 kJ·mol^{-1}. The net energy difference for two molecules is $\Delta G_d = 2(\mu^0_1 - \mu^0_2)$ and the result will depend on the molecules' arrangement in the aggregate.[42] For a linear aggregate of N molecules $\Delta\mu_N^0 = \Delta\mu_\infty^0 + \alpha/N$, and thus for two molecules $\Delta G_d = -\alpha = 47$ kJ·mol^{-1}. For a disk-like aggregate, $\Delta\mu_N^0 = \Delta\mu_\infty^0 + \alpha/\sqrt{N}$, thus $\Delta G_d = -\alpha(2 - 2^{1/2}) = 28$ kJ·mol^{-1}. If similar estimates are made using CMC for the full length of PEG linkers[41] (approximately 80 EO units, $X_{CMC} = 2.6 \times 10^{-3}$), the resulting energy difference ranges from 9 to 15 kJ·mol^{-1} for the disk and linear aggregates, respectively. The measured value of the activation energy is much closer to the value for the tail-less hydrocarbon heads indicating that PEG tails do not contribute significantly to the activation energy and that in the molecular interpretation of the measured dissociation rate the effect of linkers on the activation energy can be disregarded.

Temperature Dependence. Temperature dependence of hydrophobic interactions was measured in the temperature range from 15 to 40 °C with a constant probe velocity of 1000 nm/s. The most probable rupture forces were determined by fitting the force histograms by Gaussian curves. An alternative method to determine the most probable force is by fitting the experimental histogram of rupture forces to the probability density function[43] and finding maximum of the distribution according to the following equations:[44,45]

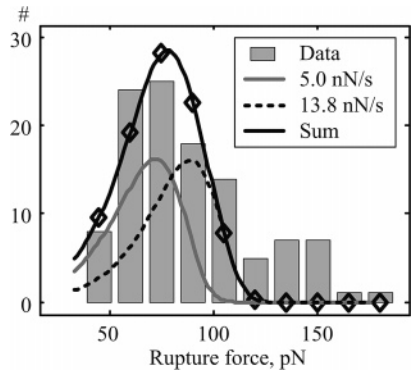

Figure 4. The figure shows the histogram of forces collected at 20 °C with fit by the sum of two probability density functions that use different experimentally measured loading rates. All measured loading rates are represented by two averaged values. These values are given in the legend and represent averages of low and high loading rates measured in experiment with constant probe velocity.

$$p(F) = \frac{K_d^0}{r}\exp\left[\frac{Fx^{\ddagger}}{k_BT} - \frac{K_d^0}{r}\frac{k_BT}{x^{\ddagger}}(e^{F\cdot x^{\ddagger}/k_BT} - 1)\right] \quad (3a)$$

$$F^* = \frac{k_BT}{x^{\ddagger}}\ln\left[\frac{rx^{\ddagger}}{K_d^0\cdot k_B\cdot T}\right] \quad (3b)$$

Here $p(F)$ is the probability density function, K_d^0 is the dissociation rate, r is the loading rate at the rupture ($r = dF/dt$), $x^{\ddagger}$ is the barrier width, F is the rupture force, and F^* is the most probable rupture force. Figure 4 shows the histogram of the rupture forces detected at 20 °C and the fit by the sum of two distribution functions given by eq 3a calculated using two loading rates. Loading rates for the fit were obtained from the experimentally measured rates by splitting the distribution of rates into low and high loading rate sets so that both sets have the same number of data points. The averaged loading rates are given in the figure's legend. It can be noted that the most probable rupture forces in an experiment with a constant probe velocity can be noticeably different due to differences in loading rates. Similar histograms for all temperature measurements with fits by probability density function according to eq 3a are provided in the Supporting Information.

Gaussian curves determine the most probable force without regard for the range of loading rates (which are similar in the temperature-dependent experiments), and they allow comparison of the most probable forces detected under identical conditions in the same graph. Figure 4 shows the most probable rupture forces collected using two different sets of samples and probes at different temperatures ranging from 15 to 40 °C. Both data sets give similar forces that do not show significant temperature dependence. Absence of strong temperature dependence is not surprising considering moderate changes in the oil−water interfacial energy in this temperature range[46] as well as temperature dependence of the free energy of hydration of small alkane molecules.[47,48]

The detected temperature dependence can be compared with the empirical equation of state that describes the temperature dependence of the free-energy of hydration for hydrocarbons.[48] When comparing results of this model with the experimental

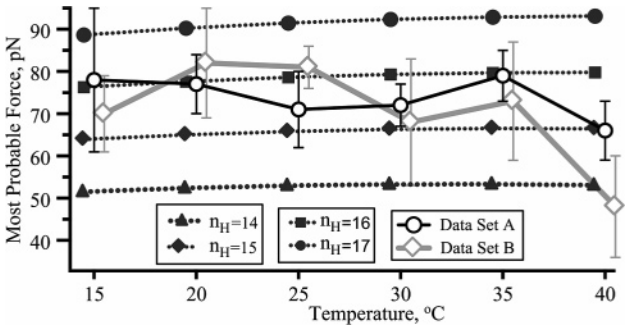

Figure 5. Figure shows the most probable rupture force between hexadecane molecules as a function of temperature for two sets of data. Two solid curves with open-face symbols correspond to two data sets collected with different samples and probes. Error bars indicate the fit error[28] of the force histogram by Gaussians. Dotted lines with solid symbols show the estimates of forces corresponding to the hydration of between 14 and 17 hydrogens (indicated in the legend). Force estimates are calculated using eq 5. These calculated curves demonstrate that for the temperature-independent barrier width and constant number of hydrogens hydrated upon dissociation, variation in the most probable forces is expected to be small.

results obtained here, it will be assumed that the temperature dependence of the activation free-energy $\Delta G^{\ddagger}$ of alkane's dissociation stems from the temperature dependence of the free-energy of hydration. The temperature dependence of the free-energy of hydrophobic solvation in water will be used here to estimate how the most probable force changes with temperature. The free energy of hydration is given by the empirical model[48] as follows:

$$\Delta G = (T/T^*)\Delta G^{\circ}_{T^*} - \Delta C^{\circ}_p[T \ln(T/T^*) + T^* - T]$$

$$\Delta C^{\circ}_p = 0.033 n_H [\mathrm{kJ \cdot mol^{-1} \cdot K^{-1}}] \quad (4)$$

$$\Delta G^{\circ}_{T^*} = 6.4 + 1.85 n_H \, [\mathrm{kJ \cdot mol^{-1}}]$$

Here T^* is the temperature ($\sim$290$-$300 K) where the enthalpy of a hydrocarbon solution in water is zero and n_H is the number of hydrated hydrogens in the hydrocarbon molecule. Increase in ΔG with temperature is typical for hydrophobic interactions.[47] Substituting eq 4 into Arrhenius' equation, the most probable force can be calculated as

$$F^* = \frac{k_B T}{x^{\ddagger}} \ln\left[\frac{r x^{\ddagger}}{f k_B T}\right] + \frac{\Delta C^{\circ}_p(n_H)((1 + \ln[T^*/T])T - T^*) + \Delta G^{\circ}_{T^*}(n_H)T/T^*}{x^{\ddagger} N_A} \quad (5)$$

To demonstrate the weak temperature dependence over the experimental range of temperatures, a calculated set of F^* is included in Figure 5. Calculated points are according to eq 5 above, and use the value for the barrier width $x^{\ddagger}$ of 0.24 nm, as determined above from the loading rate dependence. The other variables, such as temperature and loading rate, are taken to be the same as in experimental measurements. The Arrhenius' preexponential factor (f) was taken to be 10^7 as explained above.[33] Force vs temperature dependencies shown in Figure 5 indicate that the measured forces correspond to hydration of from 14 to 17 hydrogens, which is approximately a quarter of the total number of available hydrogens (76 from two hexadecane molecules). Not surprisingly, this number agrees with the earlier conclusion that approximately one-quarter of the hexadecane surface gets hydrated upon forced dissociation, and thus it is consistent with a nonglobular conformation of hexadecane in the dimeric state in water. This suggestion agrees with the measured linearity of the free-energy of transfer of *n*-alkyl chain carboxylic acids from the organic phase into aqueous buffer[39] as well as with the results of molecular dynamics simulations that suggest that hydrocarbons in water might adopt globular conformations only for very long linear chains.[37]

Conclusion

The described method expands the scope of single molecule force spectroscopy, making it possible to probe single molecule interactions between highly insoluble (i.e., hydrophobic) molecules. Use of a shorter hydrophilic polymer to cover the surfaces under the tether-attached hydrophobic molecules is shown to activate the interaction, leading to a sharp increase in the detection of the double-tether events. Statistical analysis of the loading rate dependence of rupture forces yields a barrier width of 0.24 nm. This barrier width is close to the values predicted by molecular dynamics simulations for larger hydrophobic species such as fullerenes.[30] The dissociation rate is used to estimate the activation energy, $\Delta G^{\ddagger} = 41 \pm 6$ kJ mol^{-1}. This value is noticeably lower than the estimates that can be made based on the free energy of cavitation in water[17,34] and agrees with the estimates based on the critical micellar concentration of alkyl ethoxide surfactants.[40] The latter comparison indicates that the PEG linker does not significantly participate in the measured interactions. Finally, it is estimated that approximately one-quarter of the surface of hexadecane molecule hydrates upon forced dissociation from the dimeric state. This is consistent with an unentangled side-by-side arrangement of molecules in the dimer.

Acknowledgment. We thank Duke University and NSF (BES-05-08284) for financial support and Dor Ben-Amotz for his comments on this work.

Supporting Information Available: Detailed description of the data manipulation as well as histograms of force data for the temperature-dependent studies of rupture forces are provided. This material is available free of charge via the Internet at http://pubs.acs.org.

References and Notes

(1) Blokzijl, W.; Engberts, J. *Angew. Chem., Int. Ed. Eng.* **1993**, *32*, 1545.
(2) Dill, K. A. *Biochemistry* **1990**, *29*, 7133.
(3) Oas, T. G.; Toone, E. J. *Adv. Biophys. Chem.* **1997**, *6*, 1.
(4) Scheraga, H. A. *J. Biomol. Struct. Dyn.* **1998**, *16*, 447.
(5) Tanford, C. *Science* **1978**, *200*, 1012.
(6) Chandler, D. *Nature* **2005**, *437*, 640.
(7) Widom, B.; Bhimalapuram, P.; Koga, K. *Phys. Chem. Chem. Phy.* **2003**, *5*, 3085.
(8) Ashbaugh, H. S.; Pratt, L. R.; Paulaitis, M. E.; Clohecy, J.; Beck, T. L. *J. Am. Chem. Soc.* **2005**, *127*, 2808.
(9) Ball, P. *Nature* **2003**, *423*, 25.
(10) Yaminsky, V.; Ohnishi, S. *Langmuir* **2003**, *19*, 1970.
(11) Evans, D. R.; Craig, V. S. J.; Senden, T. J. *Physica A* **2004**, *339*, 101.
(12) Maczynski, A.; Wisniewska-Goclowska, B.; Goral, M. *J. Phy. Chem. Ref. Data* **2004**, *33*, 549.
(13) Christenson, H. K.; Claesson, P. M. *Adv. Colloid Interface Sci.* **2001**, *91*, 391.
(14) Doshi, D. A.; Watkins, E. B.; Israelachvili, J. N.; Majewski, J. *Proc. Nat. Acad. Sci. U. S. A.* **2005**, *102*, 9458.
(15) Fa, K. Q.; Nguyen, A. V.; Miller, J. D. *J. Phys. Chem. B* **2005**, *109*, 13112.
(16) Ray, C.; Akhremitchev, B. B. *J. Am. Chem. Soc.* **2005**, *127*, 14739.
(17) Ben-Amotz, D. *J. Chem. Phys.* **2005**, *123*, 184504. Note that the coefficients of the C-EOS which are listed in Table 3 of this reference require using R_c (nm) and β (mol/kJ) on the right-hand-side of eq A2.

(18) Ratto, T. V.; Langry, K. C.; Rudd, R. E.; Balhorn, R. L.; Allen, M. J.; McElfresh, M. W. *Biophys. J.* **2004**, *86*, 2430.
(19) Longo, G.; Szleifer, I. *Langmuir* **2005**, *21*, 11342.
(20) Chen, C. C.; Dormidontova, E. E. *Langmuir* **2005**, *21*, 5605.
(21) Sulchek, T. A.; Friddle, R. W.; Langry, K.; Lau, E. Y.; Albrecht, H.; Ratto, T. V.; DeNardo, S. J.; Colvin, M. E.; Noy, A. *Proc. Nat. Acad. Sci. U. S. A.* **2005**, *102*, 16638.
(22) Hinterdorfer, P.; Gruber, H. J.; Kienberger, F.; Kada, G.; Riener, C.; Borken, C.; Schindler, H. *Colloids Surf., B* **2002**, *23*, 115.
(23) Hermanson, G. T. *Bioconjugate Techniques*; Academic Press: New York, 1996.
(24) Proksch, R.; Schaffer, T. E.; Cleveland, J. P.; Callahan, R. C.; Viani, M. B. *Nanotechnology* **2004**, *15*, 1344.
(25) Oesterhelt, F.; Rief, M.; Gaub, H. E. *New J. Phys.* **1999**, *1*, 6.1.
(26) Friedsam, C.; Wehle, A. K.; Kuhner, F.; Gaub, H. E. *J. Phys.: Condens. Matter* **2003**, *15*, S1709.
(27) Evans, E.; Ritchie, K. *Biophys. J.* **1999**, *76*, 2439.
(28) Bevington, P. R.; Robinson, D. K. *Data Reduction and Error Analysis for the Physical Sciences*, 2 ed.; McGraw-Hill: New York, 1991.
(29) Pratt, L. R.; Chandler, D. *J. Chem. Phys.* **1977**, *67*, 3683.
(30) Choudhury, N.; Pettitt, B. M. *J. Am. Chem. Soc.* **2005**, *127*, 3556.
(31) Li, L. W.; Bedrov, D.; Smith, G. D. *J. Chem. Phys.* **2005**, *123*, 204504.
(32) Rajamani, S.; Truskett, T. M.; Garde, S. *Proc. Nat. Acad. Sci. U. S. A.* **2005**, *102*, 9475.
(33) Lapidus, L. J.; Eaton, W. A.; Hofrichter, J. *Proc. Nat. Acad. Sci. U. S. A.* **2000**, *97*, 7220.
(34) Hofinger, S.; Zerbetto, F. *Chem. Soc. Rev.* **2005**, *34*, 1012.
(35) Lepori, L.; Gianni, P. *J. Solution Chem.* **2000**, *29*, 405.
(36) Benamotz, D.; Herschbach, D. R. *J. Phys. Chem.* **1990**, *94*, 1038.
(37) Mountain, R. D.; Thirumalai, D. *Proc. Nat. Acad. Sci. U. S. A.* **1998**, *95*, 8436.
(38) Tanford, C. *The Hydrophobic Effect: Formation of Micelles and Biological Membranes*, 2 ed.; Wiley: New York, 1980.
(39) Smith, R.; Tanford, C. *PNAS* **1973**, *70*, 289.
(40) Kumar, N.; Tilton, R. D. *Langmuir* **2004**, *20*, 4452.
(41) Huibers, P. D. T.; Lobanov, V. S.; Katritzky, A. R.; Shah, D. O.; Karelson, M. *Langmuir* **1996**, *12*, 1462.
(42) Israelachvili, J. N. *Intermolecular and Surface Forces*, 2 ed.; Academic Press: New York, 1991.
(43) Evans, E. *Annu. Rev. Biophys. Biomol. Struct.* **2001**, *30*, 105.
(44) Strunz, T.; Oroszlan, K.; Schumakovitch, I.; Guntherodt, H. J.; Hegner, M. *Biophys. J.* **2000**, *79*, 1206.
(45) Evans, E.; Ritchie, K. *Biophys. J.* **1997**, *72*, 1541.
(46) Zeppieri, S.; Rodriguez, J.; de Ramos, A. L. L. *J. Chem. Eng. Data* **2001**, *46*, 1086.
(47) Baldwin, R. L. *Proc. Nat. Acad. Sci. U. S. A.* **1986**, *83*, 8069.
(48) Gill, S. J.; Wadso, I. *Proc. Nat. Acad. Sci. U. S. A.* **1976**, *73*, 2955.